DFT Based Modeling of Asymmetric Non-Fullerene Acceptors for High-Performance Organic Solar Cell

Noureen Kanwal
University of Education
Riaz Hussain
University of Education
Abdul Satar
University of Education
Mohammed A. Assiri
King Khalid University
Muhammad Imran
King Khalid University
Ajaz Hussain
Bahauddin Zakariya University
Mirza Arfan Yawer
University of Education
Riaz Hussain
University of Okara
Muhammad Yasir Mehboob (yasirbhatti587@gmail.com)
University of Okara https://orcid.org/0000-0002-7143-1129
Muhammad Khalid
Khwaja Fareed University of Engineering & Information Technology
Khurshid Ayub
COMSATS Institute of Information Technology - Abbottabad Campus

Research Article

Keywords: polymer solar cells, Frontier molecular orbital analysis, electron-withdrawing properties

Posted Date: January 12th, 2022

DOI: https://doi.org/10.21203/rs.3.rs-1121568/v1

Abstract

Abstract

Five new asymmetric NFA-based polymer solar cells i.e., **N1-N5** are designed by doing modification in terminal groups of the acceptor part of experimentally synthesized reference molecule with (4,4,9,9-tetramethyl-4,9 dihydroselenopheno [2',3':5,6]-s-indaceno [1,2-b] thiophene) core. Frontier molecular orbital analysis is used to study their photovoltaic and optoelectronic properties. It confirmed the electrons' transportation from the donor to the acceptor part. It stated that all molecules have a lower bandgap than **R** and **N2** has the lowest bandgap of 2.01 eV. The molecular orbital potential analysis confirmed the electron-withdrawing properties of the terminal groups. Optical properties studies evaluated maximum absorption with transition energies. All newly designed molecules **N1-N5** show higher λ_{max} values than **R** i.e., in the range of 680-740 nm with **N2** having the highest λ_{max} of 735 nm and lowest transition energy of 1.69 eV. Dipole moment studies showed that **N3** has a maximum dipole moment of 7-40 D with all others having comparable values. TDM plots confirmed the electron shifting from donor to acceptor region. Reorganization energy analysis showed that **N1** and **N3** have the lowest reorganization energy values thus giving the highest electron mobilities. V_{oc} calculated results of all molecules **N1-N5** have lower values than **R** when coupled with **PTB7-Th** donor polymer. Charge transport analysis of **N2** and PTB7-Th coupled molecule confirmed the acceptor type nature of our designed molecules.

Highlights

1. **Asymmetric** fullerene free acceptor molecules (**N1-N5**) are studied for organic solar cells applications.
2. Significant lowering of energy gap with concomitant red shifting of the absorption spectra is achieved with end-group engineering**.**
3. The acceptors molecules show lower binding energy and excellent electron and hole reorganizational energies.
4. All acceptor molecules have remarkable optoelectronic properties compared to reference **R**.

1. Introduction

Non-fullerene-based acceptors have gained major attention from researchers in the field of polymer solar cells nowadays. This is mainly because of better light absorption ability in wider spectral range and easily modifiable structure i.e., donor part, acceptor part, and side chains to tune energy levels and impart desirable characteristics in them as compared to fullerene-based acceptors which are not easily modifiable. There are two major classes of non-fullerene acceptors i.e., symmetrical NFAs and asymmetrical NFAs. Symmetrical NFAs with the basic structural type of Acceptor-Donor-Acceptor containing electron-rich core with symmetrical acceptor terminal parts on both sides have got a significant position in PSCs with proficient PCEs of 17% or above. [1–4]

Asymmetric NFAs have attained a level up attention than symmetric NFAs because of their stronger intermolecular forces and higher dipole moments leading to better π-π stacking and improved dielectric constant with better charge separation, respectively. Symmetrical NFAs can be made asymmetrical by either changing the acceptor-based terminal groups on the sides of the core or modifying the core unit by imparting a different atom in it. Till time asymmetrical NFAs in polymer solar cells have attained an efficiency of 15.3% compared to PCE got from its relative symmetrical **Y6** based PSC. [5] Indaceno-dithiophene (IDT) is mostly used donor core in symmetric PSCs. In IDT replacement of the sulfur atom in thiophene ring with selenium atom to make it a selenophene ring which makes it a more electron-donating core with reduced aromaticity than thiophene. It increased the conjugation by increasing molecular orbital overlap to decrease the energy gap between them and improve the solid-state packing in this non-fullerene-based acceptor.[6]

NFAs containing Indacenodiselenophene (IDSe) have shown improved optical properties in OSCs [7–11]. Replacement of one of thiophene with selenophene in IDT gave asymmetric core SePT. When this asymmetric core is given terminal groups with 2-(3-oxo-2,3-dihydro-1H-cyclopenta[b]naphthalen-1-ylidene) malononitrile (IN) terminal groups, these molecules gave improved flexibility in molecular orbitals and better absorption properties. It showed a PCE value of 10.29% when blend with PM6 polymer donor. [12]

These results were taken as an encouragement to take synthesized SePT based asymmetric NFA and modify its terminal groups by introducing new end-capped groups to get better optical and photovoltaic properties. Five new NFAs are introduced **N1-N5** using this asymmetric core with symmetrical terminal groups **D1-D5** with modified end-capped groups respectively. By changing terminal groups on the acceptors part and using density functional theory for analysis, we tend to improve conversion efficiencies, stability, and electronic transitions relative to the reference **R**. Moreover, the acceptor-based nature of these molecules was proven by making a blend of the most efficient designed molecule with **PTB7-Th** polymer donor to study the electronic flow from the donor to the acceptor region.

2. Computational Methodology

The systematical analysis is done using Gaussian 09W [13] and the outcomes are anticipated through Gauss View 5.0. For structural optimization of reference molecule with restriction-free symmetry, theory level DFT along with level i.e. 6-31G(d,p) is used with four various functional i.e. B3LYP [14], CAM-B3LYP [15], ωB97XD [16], and MPW1PW91 [17]. For identification of the best computational method, the absorption maximum wavelength of the reference molecule is measured using above mentioned four functionals and then are compared with its experimental UV data. λ_{max} calculation of reference molecule and all newly fabricated molecules is done using Chloroform as solvent.

Frontier molecular orbital approach, the partial density of states (PDOS), transition density matrices (TDM), dipole moment analysis, and molecular electrostatic potential (MEP) analysis are done using B3LYP along with same above-mentioned level at DFT level. Along with this analysis, reorganization energy calculation of holes and electrons is also done. It has two classes, one is internal reorganization

energy (λ_{int}) and the other is external reorganization energy (λ_{ext}) demonstrating modifications in internal geometry and impact of external stimuli, respectively. As the impact of external stimuli is very little, thus it is neglected. To calculate the reorganization energy of electrons (λ_e) and holes (λ_h), the equations given below are useful. [18]

$$\lambda_e = \left[E_0^- - E_-\right] + \left[E_-^0 - E_0\right]$$

$$\lambda_h = \left[E_0^+ - E_+\right] + \left[E_+^0 - E_0\right]$$

E_-^0 and E_+^0 represents neutral molecule's energies through the optimized structures of anions and cations respectively while E_- and E_+ are energies of optimized anions and cations using the neutral molecule. E_0^- and E_0^+ represent single point energies of anions and cations while E_0 is neutral molecule's single point energy on the lowest energy state.

3. Results And Discussion

In the current study, the reference molecule was [19] was modified with different end-capped groups and in this way five freshly fabricated molecules **N1-N5** are obtained. Absorption maximum wavelength of reference molecule is obtained after its optimization using level DFT 6-31G(d,p) on four chosen functionals i.e. B3LYP, CAM-B3LYP, ωB97XD, and MPW1PW91. The λ_{max} values obtained on these functionals are 682, 532, 514, and 646 nm, respectively. The computationally obtained λ_{max} on B3LYP functional matched precisely to the experimental data of reference which is 682 nm. It can also be seen through Figure 1 showing the comparison between the maximum absorption wavelengths obtained computationally and experimental data. This also justifies the use of B3LYP functional for further computational analysis done on the newly designed molecules **N1-N5**.

3.1 Frontier molecular orbital analysis

The two-dimensional structure of the reference molecule and newly modified acceptor groups are shown in Figure 2. FMO analysis demonstrates the optical properties of reference molecules and newly tailored molecules. It related the energies of both HOMO and LUMO [20]. HOMO and LUMO of **R** and newly fabricated molecules obtained through FMO analysis are shown in Figure 3. HOMO influences the bonding properties while LUMO influences the anti-bonding properties in NFA molecules on the ground state and excited state. [21] If stronger electron-withdrawing groups are present within the acceptor part of the molecule then it helps to increase the λ_{max} value. A molecular orbital having higher or lower energy also determines its stability. The more stable a molecular orbital is the more ease of electronic transportations throughout the excitation process [22].

A less stable filled HOMO plays a more effective role in electronic excitation than a more stable HOMO. It is more effective to have LUMO of higher energy along with HOMO of higher energy to have maximum absorption of solar photons for electronic excitations. [23] The LUMO should be stable enough to hold the transported electrons during the excitation process for more time and competently. The acceptor region is the LUMO in PSCs which if perfectly tuned can be useful in capturing more photons and effectively converting them into electric signals to make SCs more proficient. The electronic transportation rate between HOMO and LUMO is directly related to the percentage of electronic transitions in an excited molecule [19].

The graphic representation of molecular orbitals of R and newly fabricated molecules are shown in figure 3.

HOMO describes where the electronic population is present in the donor part of the solar cell. Whereas LUMO elaborates the possibility of transportation of electronic population towards the acceptor region of SCs. The more electron capturing ability the acceptor part has, the more it can make the electrons get transported towards the acceptor part from the donor part. In the current study, the HOMO of the reference molecule and all newly designed molecules are identical, showing the presence of an electronic population on the donor region of the SCs. However, the LUMO graphs show that the electronic density is distributed all over the molecule but is denser on the acceptor groups. In **N1**, the LUMO graph shows that the electronic population is spread all over but is richer on one side of the molecule. **N2** LUMO shows electron density present all over the molecule but most of this density is accumulated on both acceptor sides of the molecule. In **N3**, **N4**, and **N5** the electron population is present all over the molecules but is denser on the acceptor regions.

Thus, these outcomes proved the electron-deficient nature of the acceptor groups, and the best electronic flow from the donor part towards the acceptor part is shown by **N2** because of the stronger electron capturing effect of its end capped groups i.e., dinitro and thiochloro groups. The computational calculations give us data about the E_{HOMO} and E_{LUMO} and of R and newly fabricated molecules N1-N5 which is displayed in Table 1.

Table 1
Energies of HOMO, LUMO, and band gap E_g of **R** as well as **N1-N5**

Molecules	HOMO energy (eV)	LUMO energy (eV)	E_g
R	-5.62	-3.48	2.14
N1	-5.85	-3.83	2.02
N2	-5.74	-3.73	2.01
N3	-5.84	-3.79	2.05
N4	-5.69	-3.57	2.12
N5	-5.77	-3.69	2.08

These calculations revealed that the energies of HOMO and LUMO of newly fabricated molecules are lower than that of **R**. The increase in energy is due to the increase in conjugation in acceptor sides connected to an asymmetric central unit. This also caused an increase in absorption maxima. Reduced the E_{HOMO} and E_{LUMO}, reduced are the energy losses and improved open-circuit voltage which plays a vital role to facilitate electronic transitions to give better efficiencies. [24, 25]

The energy of HOMO of the reference and five newly fabricated molecules are shown in an increasing order **N1< N3< N5< N2< N4< R**. While the increasing order of LUMO energy of reference and newly fabricated molecules is **N1< N3< N2< N5< N4< R**. As is clear that the most minimum energies of molecular orbitals are shown by N1 because of stronger electron capturing end-capped groups i.e., two dicyano groups and improved conjugation. It is followed by **N3** containing one acid and three cyano groups on terminal parts which makes it more electron-deficient and stronger electron-withdrawing acceptor moiety than **N2** (one thiochloro and dinitro end-capped groups), **N5** (two acid and dicyano end-capped groups), and **N4** (dicyano and dichloro groups). The highest values of E_{HOMO} and E_{LUMO} are displayed by **N4** when compared to all newly fabricated molecules which are caused to relatively less strong electron capturing end-capped groups.

The energy band gap of **R** and the newly tailored molecules is shown below in decreasing order **R >N4 >N5 >N3 >N1 >N2**. The energy bandgap is the difference between E_{LUMO} and E_{HOMO}. By comparing the energy band gap exhibited by all newly fabricated molecules and **R** molecules, we deduced that the energy band gap of **N1-N5** molecules is smaller than the **R** molecule because of the more electron-withdrawing effect influenced by the terminal groups. The least energy band gap is displayed by the **N2** molecule that has an acceptor region containing dichloro and thiochloro functional groups. **N1** has a higher bandgap than **N2** but lesser than **N3, N5**, and **N4** because of its two dicyano groups. **N3** containing one acid and three cyano groups in acceptor moiety exhibits a greater energy band gap than **N2** and **N1**. **N3** is followed by **N5** (two acid and dicyano electron-withdrawing groups), and **N4** (dicyano and dichloro terminal groups). The bar chart representation of E_{LUMO} and E_{HOMO}, and their difference (E_g) is shown in Figure 4.

The FMO studies gave us conclusion that all the newly fabricated molecules **N1-N5** shows better electron capturing nature than **R**. And among all the newly fabricated molecules, most appropriate results are displayed by **N2** making it a good choice to give a proficient SCs.

3.2 Partial density of states

The partial density of states (PDOS) technique relates the bonding, anti-bonding atoms, and molecular orbitals. The PDOS graphs of reference and newly fabricated molecules **N1-N5** are displayed in figure 5. From the graphs, the change in terminal groups of acceptor parts shifted the electronic density towards itself. The overall study of the electronic distribution revealed that all the new NFAs showed proficient electronic distribution along with improved charge transportation from the donor part of the SCs to the acceptor part relative to the **R** molecule.

This technique is used for further clarifying the results obtained from FMO analysis. The density of states calculations of reference and all newly fabricated molecules are done on the same functional level B3LYP using a basis set 6-31G(d,p). The left side of the PDOS plots symbolizes the HOMO region while the right side is symbolizing the LUMO region of **R** and **N1-N5** molecules. The red lines characterize the comparative intensity of the donor part while the green lines are of the acceptor part. The HOMO of all the fabricated molecules shows that the electronic population is mainly on the core unit while in the LUMO, this electronic population is shifted on the acceptor region more than the reference molecule. The proficient electronic intensity transition of reference and all the newly designed molecules are shown in decreasing order **N2 >N3 >N5 >N1 >N4 >R.**

3.3 Molecular Electrostatic Potential (MEP)

Molecular electrostatic potential analyzes the electron's distribution in the molecule indicating its electron-deficient and electron-rich regions. [26] MEP plots of reference and newly fabricated molecules **N1-N5** are shown in Figure 6. The molecules are colored showing different regions according to electronic distribution and the scale indicates how electronic distribution relates to the colors.

Three major colors are present in the plots as well as in scales i.e., red, blue, and green which indicates an abundance of positive charge, an abundance of a negative charge, and a neutral region respectively. The reference and all newly fabricated molecules N1-N5 showed a similar trend in MEP plots indicating the donor part in blue color showing its electron-rich and electron-donating nature while the acceptor end-capped groups are in red proving their electron-deficient and electron-withdrawing nature.

3.4 Optical Properties

Optical properties of **R** and newly fabricated molecules **N1-N5** are analyzed using TD-SCF with basis set 6-31G(d,p) and solvent chloroform along with model CPCM. This analysis gives information about the absorption maximum in the electromagnetic spectrum. [27] Optical properties include maximum absorption wavelength (nm), transition energy (eV), oscillation strength (*f*), and major contributing orbitals.

The wavelength of maximum absorption (λ_{max}) of **R** and new fabricated molecules **N1-N5** are 682, 729, 735, 714, 696, and 708 nm respectively. All newly tailored molecules have greater λ_{max} as compared to **R** while all the values are within visible spectral range with **N2** having the highest λ_{max} value due to electron-withdrawing effect caused by thiochloro group along with dinitro group present in its acceptor moiety. It is followed by **N1, N3, N5**, and **N4** respectively. **N1** shows higher λ_{max} than **N3, N5**, and **N4** due to the presence of two dicyano groups in its acceptor part. The difference in acceptor groups of **N1** and other molecules with lower λ_{max} is that in **N3** one cyano group is replaced by an acid group, in **N5** two cyano groups are replaced by two acid groups while in **N4** two cyano groups are replaced by two chloro groups. The increase in absorption maximum is known as redshift. The difference between λ_{max} of newly fabricated molecules from the reference molecules gives us the value of the red shift shown by our designed molecules. The redshift shown by **N1-N5** compared to **R** is 47, 53, 32, 14, and 26 nm respectively. It is clear from this difference that acceptor groups **D1-D5** present on molecules **N1-N5** show more electron-withdrawing properties and among all these newly fabricated molecules, **N2** is showing maximum redshift.

Excitation energy is also known as transition energy is also an important optical property that defines the charge transportation trend in the desired molecules. Smaller excitation energy makes the faster electronic transition from HOMO to LUMO making the molecules have greater charge mobilities and conversion efficiencies. In our study, all the tailored molecules have smaller transition energy than **R** which makes them have higher charge mobilities and PCE values than that of the **R** molecule. **N2** has the lowest excitation energy value than the other tailored molecules i.e., 1.69 eV followed by **N1** (1.70 eV), **N3** (1.73 eV), **N5** (1.75 eV), and **N4** (1.78 eV), respectively as shown in Table 2. Thus, it is concluded that **N2** molecule having **D2** terminal group is proved to be the best choice among the newly fabricated molecules while all the **N1-N5** NFAs show better results than the reference molecule.

Table 2
The computationally calculated and experimentally recorded λ_{max} (nm), Excitation energy (eV), oscillator strength, major contribution of molecular orbitals

Molecules	Calculated λ_{max} (nm)	Experimental λ_{max}(nm)	Energy (eV)	Osc. Strength (*f*)	Assignment	Dipole Moment
R	682	682	1.82	2.1932	HOMO→LUMO (99%)	6.71
N1	729	---	1.70	1.8572	HOMO→LUMO (98%)	6.87
N2	735	---	1.69	1.8184	HOMO→LUMO (98%)	3.60
N3	714	---	1.73	2.0238	HOMO→LUMO (98%)	7.40
N4	696	---	1.78	2.0189	HOMO→LUMO (98%)	7.07
N5	708	---	1.75	1.9664	HOMO→LUMO (98%)	5.44

3.5 Dipole Moment

The dipole moment is an important factor having a great effect on the efficiency of PSCs. Systematically calculated dipole moment values of **R** and **N1-N5** molecules have been shown in Table 2.

It gives information about the solubility of the investigated molecule in an organic solvent i.e., chloroform in our case. A higher dipole moment indicates greater solubility in the solvent. The **N3** molecule has the highest dipole moment of 7.40 D followed by **N4, N1, R, N5**, and **N2** respectively. Greater dipole moment helps molecules to be self-arranged for better charge mobilities.

3.6 Reorganization Energy

Reorganization energy is used for the systematic calculation of electrons and holes mobilities. The holes and charge mobilities calculated systematically help in elaborating the working of SCs. Charge mobility has an inverse relation with reorganization energy in a way that the greater the reorganization energy smaller the charge mobilities. This depends on many aspects including structural properties of anions and cations.

The geometry of anion defines the transportation of electrons from a donor while the geometry of cations describes the hole accumulation in the acceptor part of SCs. So, reorganization is used to study the electron transportation between the donor and acceptor. It is categorized into two classes i.e., external,

and internal reorganization energy. We focused only on the latter type and neglected the external reorganization energy because of no environmental factor affecting investigated molecules.

Reorganization energy calculations as shown in Table 3 revealed that **N1** and **N3** showed the lowest energy values which makes these two molecules have the highest electron mobilities. All other molecules show comparable results.

Table 3
Reorganization energy of electrons and holes of **R** and **N1-N5** calculated at B3LYP, 6-31G(d,p) level of DFT

Molecules	λ_e (eV)	λ_h (eV)
R	0.0087	0.0069
N1	0.0073	0.0074
N2	0.0119	0.0076
N3	0.0075	0.0091
N4	0.0091	0.0076
N5	0.0094	0.0084

3.7 Transition Density Matrix and Binding Energy

The transition density matrix technique is utilized for assessing the electronic transitions within the reference and newly fabricated molecules (**N1-N5**). It is done also on the same functional as above i.e. B3LYP with basis set 6-31G(d,p). As hydrogen atoms have little effect on transition, so it was neglected. The TDM graphs of R and new molecules **N1-N5** are displayed in Figure 7.

TDM analysis is used to study the excitations, electron-hole localization, and relation between the donor and acceptor part within the molecule. For this study, we differentiated the reference and newly designed molecules into two main parts i.e., donor and acceptor region. It can be seen through the plots that the holes and electrons of exciton are accumulated in the donor and acceptor region respectively. In **R** and **N1-N5** molecules, most of the electron density is accumulated in the acceptor region with a little density on the donor part. This proved that the electronic transportation from the donor region to the acceptor region is improved efficiently by fabricating the end-capped groups within the SCs.

Binding energy (E_b) is an important factor influencing dissociation potential thus affecting the performance of a polymer solar cell. Binding energy has an inverse relation with charge mobilities. Molecules having greater binding energies have lower charge mobilities and lower current densities. This analysis is used to relate the Columbic force among the holes and electrons in a molecule. This

interaction between holes and electrons is directly dependent upon the binding energy and binding energy is inversely dependent upon exciton breakdown in an excited state. Thus, it is concluded that greater forces of attraction between holes and electrons lead to higher columbic forces leading to higher binding energies causing smaller exciton dissociation energy at the excited state. The below-mentioned equation has been used to calculate the binding energies of R and newly fabricated molecules **N1-N5**. [28]

$$E_b = E_{H-L} - E_{opt}$$

3

E_{H-L} is band gap between the bonding and anti-bonding molecular orbital, E_{opt} is minimum first excitation energy. The binding energies of R and all the newly fabricated molecules are tabulated in Table 4. All the molecules show relatively smaller binding energies making them efficient molecules.

Table 4
Band gap(eV), excitation energy (eV), and Binding energy values of **R** and **N1-N5**

Molecules	E_{H-L}	E_{opt}	E_b
R	2.14	1.82	0.32
N1	2.02	1.70	0.32
N2	2.01	1.69	0.32
N3	2.05	1.73	0.32
N4	2.12	1.78	0.34
N5	2.08	1.75	0.33

3.8 Open Circuit Voltage

Open circuit voltage is significant for evaluating the SC's efficiency. When light falls on SCs, the electron gets excited from the donor's HOMO to the donor's LUMO. Then this electron moves from the donor's LUMO to the acceptor's LUMO. Open circuit voltage (V_{oc}) is the difference between E_{HOMO} of the donor and E_{LUMO} of the acceptor. It is also shown below in equation form.

$$V_{OC} = \left(E^{D}_{HOMO} - E^{A}_{LUMO}\right) - 0.3$$

4

All our new molecules N1-N5 are NFA based, so we calculated the V_{OC} using commonly used polymer donors i.e., PTB7-Th. The outcomes can be visualized in Figure 8. For more charge transportation from

donor to an acceptor molecule, the energies of HOMO and LUMO play a significant role. HOMO with higher energy and LUMO with lower energy facilitate more charge transportation. [29]

3.9 Charge Transfer (CT) analysis through N2/PTB7-Th Complex

All newly fabricated molecules are acceptor type thus for the charge transfer analysis, we used PTB7-Th polymer donor. As the **N2** acceptor molecule is proved to be the best choice among all newly fabricated molecules due to its lowest bandgap along with higher λ_{max}, therefore we used this **N2** molecule for CT analysis. The optimization of PTB7-Th and **N2** complex was done on DFT along B3LYP with a basis set 6-31G(d,p). The interface interaction suggested that the electron population is on the boundary of acceptor and donor maximizing the charge transfer within the complex. The optimized structure is displayed in Figure 9. [30]

The charge distribution in the molecular orbitals is also studied at function B3LYP with basis set 6-31G(d,p). The outcomes as displayed in Figure 10 conclude that in HOMO, the donor has most of the electron population but in LUMO most of the electronic density resides on the acceptor molecule. This proves the electronic shifting from the donor part towards the acceptor part. [31–43] It also confirms the acceptor-type nature of our designed molecule **N2**.

4. Conclusion

Five novels NFAs **N1-N5** are designed by using the method of modifying the terminal groups of acceptor parts to enhance the optoelectronic and photovoltaic properties of these SCs. We used an asymmetric electron-donating core SePT with acceptor groups **D1-D5**, respectively. The systematically calculated energy, optical, and structural properties are compared with reference molecules. The FMO approach used for the investigation concluded that all the tailored molecules show better properties compared to **R** with **N2** having the highest maximum absorption wavelength, improved excitation energy with the least energy bandgap in chloroform solvent. Reorganization energy calculation revealed that all molecules have comparable energy values while **N1** and **N3** show maximum charge mobilities than holes mobilities proving them to be good electron-transporting materials. A complex of **N2** with PTB7-Th donor polymer proved its acceptor-based properties. Thus, the conclusion is that all new molecules **N1-N5** especially **N2** with improved photovoltaic properties are promising NFAs to be used in polymer solar cells.

Declarations

Conflict of interest

All authors declared no conflicts of interest.

Associated Content

Optimized Cartesian coordinates of all studied molecules (**R** and **SN1-SN9**) are available in supporting information file.

References

1. Li, G., R. Zhu, and Y.J.N.p. Yang, *Polymer solar cells.* 2012. **6**(3): p. 153-161.
2. Lin, Y. and X.J.A.o.c.r. Zhan, *Oligomer molecules for efficient organic photovoltaics.* 2016. **49**(2): p. 175-183.
3. Lin, Y. and X.J.M.H. Zhan, *Non-fullerene acceptors for organic photovoltaics: an emerging horizon.* 2014. **1**(5): p. 470-488.
4. Meng, L., et al., *Organic and solution-processed tandem solar cells with 17.3% efficiency.* 2018. **361**(6407): p. 1094-1098.
5. Pang, S., et al., *Nonfused Nonfullerene Acceptors with an A–D–A′–D–A Framework and a Benzothiadiazole Core for High-Performance Organic Solar Cells.* 2020. **12**(14): p. 16531-16540.
6. Lin, Y., et al., *An electron acceptor challenging fullerenes for efficient polymer solar cells.* 2015. **27**(7): p. 1170-1174.
7. Li, Y., et al., *Non-fullerene polymer solar cells based on a selenophene-containing fused-ring acceptor with photovoltaic performance of 8.6%.* 2016. **9**(11): p. 3429-3435.
8. Liang, Z., et al., *Near-infrared absorbing non-fullerene acceptors with selenophene as π bridges for efficient organic solar cells.* 2018. **6**(17): p. 8059-8067.
9. Wan, S.-S., et al., *Benzo [1, 2-b: 4, 5-b'] diselenophene-fused nonfullerene acceptors with alternative aromatic ring-based and monochlorinated end groups: a new synergistic strategy to simultaneously achieve highly efficient organic solar cells with the energy loss of 0.49 eV.* 2019. **7**(19): p. 11802-11813.
10. Liu, K.-K., et al., *Achieving high-performance non-halogenated nonfullerene acceptor-based organic solar cells with 13.7% efficiency via a synergistic strategy of an indacenodithieno [3, 2-b] selenophene core unit and non-halogenated thiophene-based terminal group.* 2019. **7**(42): p. 24389-24399.
11. Wan, S.-S., et al., *A bromine and chlorine concurrently functionalized end group for benzo [1, 2-b: 4, 5-b'] diselenophene-based non-fluorinated acceptors: a new hybrid strategy to balance the crystallinity and miscibility of blend films for enabling highly efficient polymer solar cells.* 2020. **8**(9): p. 4856-4867.
12. Li, C., et al., *Heteroatom substitution-induced asymmetric A–D–A type non-fullerene acceptor for efficient organic solar cells.* 2020. **40**: p. 144-150.
13. Marenich, A.V., et al., *Practical computation of electronic excitation in solution: vertical excitation model.* 2011. **2**(11): p. 2143-2161.
14. Civalleri, B., et al., *B3LYP augmented with an empirical dispersion term (B3LYP-D*) as applied to molecular crystals.* 2008. **10**(4): p. 405-410.

15. Bannwarth, C., S.J.C. Grimme, and T. Chemistry, *A simplified time-dependent density functional theory approach for electronic ultraviolet and circular dichroism spectra of very large molecules.* 2014. **1040**: p. 45-53.
16. Chai, J.-D. and M.J.P.C.C.P. Head-Gordon, *Long-range corrected hybrid density functionals with damped atom–atom dispersion corrections.* 2008. **10**(44): p. 6615-6620.
17. Fang, L., et al., *Experimental and theoretical evidence of enhanced ferromagnetism in sonochemical synthesized BiFeO 3 nanoparticles.* 2010. **97**(24): p. 242501.
18. Ans, M., et al., *Designing indacenodithiophene based non-fullerene acceptors with a donor–acceptor combined bridge for organic solar cells.* 2019. **9**(7): p. 3605-3617.
19. Liu, S., et al., *Performance of asymmetric non-fullerene acceptors containing the 4, 4, 9, 9-tetramethyl-4, 9-dihydroselenopheno [2', 3': 5, 6]-s-indaceno [1, 2-b] thiophene core.* 2021. **186**: p. 108988.
20. Ali, U., et al., *Benchmark study of benzamide derivatives and four novel theoretically designed (L1, L2, L3, and L4) ligands and evaluation of their biological properties by DFT approaches.* 2019. **25**(8): p. 1-9.
21. Benning, P., et al., *Electronic states of KxC60: insulating, metallic, and superconducting character.* 1991. **252**(5011): p. 1417-1419.
22. Maliakal, A., et al., *Photochemical stability of pentacene and a substituted pentacene in solution and in thin films.* 2004. **16**(24): p. 4980-4986.
23. Kooistra, F.B., et al., *Increasing the open circuit voltage of bulk-heterojunction solar cells by raising the LUMO level of the acceptor.* 2007. **9**(4): p. 551-554.
24. Sun, H., F. Chen, and Z.-K.J.M.T. Chen, *Recent progress on non-fullerene acceptors for organic photovoltaics.* 2019. **24**: p. 94-118.
25. Holliday, S., et al., *High-efficiency and air-stable P3HT-based polymer solar cells with a new non-fullerene acceptor.* 2016. **7**(1): p. 1-11.
26. Goszczycki, P., et al., *Synthesis, crystal structures, and optical properties of the π-π interacting pyrrolo [2, 3-b] quinoxaline derivatives containing 2-thienyl substituent.* 2017. **1146**: p. 337-346.
27. Afzal, Z., et al., *Designing indenothiophene-based acceptor materials with efficient photovoltaic parameters for fullerene-free organic solar cells.* 2020. **26**(6).
28. Adnan, M., et al., *Fine tuning the optoelectronic properties of triphenylamine based donor molecules for organic solar cells.* 2017. **231**(6): p. 1127-1139.
29. Zafar, F., et al., *End-capped engineering of truxene core based acceptor materials for high performance organic solar cells: theoretical understanding and prediction.* 2021. **53**(2): p. 1-24.
30. Khan, M.U., et al., *Designing spirobifullerene core based three-dimensional cross shape acceptor materials with promising photovoltaic properties for high-efficiency organic solar cells.* 2020. **120**(22): p. e26377.

31. Hussain, R. et al., *Efficient designing of triphenylamine-based hole transport materials with outstanding photovoltaic characteristics for organic solar cells*, 56 (2021) 5113-5131.
32. Khan, M.U, et al., *Novel W-shaped oxygen heterocycle-fused fluorene-based non-fullerene acceptors: first theoretical framework for designing environment-friendly organic solar cells*, 35 (2021) 12436-12450.
33. Mehboob, M.Y., et al., *Enhancement in the photovoltaic properties of hole transport materials by end-capped donor modifications for solar cell applications*, 42 (2021) 597-610.
34. Younas. F, et al., *Efficient Cu decorated inorganic B 12 P 12 nanoclusters for sensing toxic COCl 2 gas: a detailed DFT study*, 20 (2021) 85-97.
35. Hussain, S. et al., *Zinc-doped boron phosphide nanocluster as efficient sensor for SO2,* Journal of Chemistry, 2020 (2020).
36. Khan, M.U, et al., *Designing spirobifullerene core based three-dimensional cross shape acceptor materials with promising photovoltaic properties for high-efficiency organic solar cells*, 120 (2020) e26377.
37. Mehboob, M.Y., et al., *Designing of near-infrared sensitive asymmetric small molecular donors for high-efficiency organic solar cells*, 19 (2020) 2050034.
38. Siddique, S.S., et al., *Efficient tuning of triphenylamine-based donor materials for high-efficiency organic solar cells*, 1191 (2020) 113045.
39. Hussain, R., et al., *Molecular engineering of A–D–C–D–A configured small molecular acceptors (SMAs) with promising photovoltaic properties for high-efficiency fullerene-free organic solar cells,* 52 (2020) 1-20.
40. Ahmed, M. et al., *Benzenesulfonohydrazides inhibiting urease: Design, synthesis, their in vitro and in silico studies,* 1220 (2020) 128740.
41. Hussain, R., et al., *Density functional theory study of palladium cluster adsorption on a graphene support*, 10 (2020) 20595-20607.
42. Akram. M., et al., *End-capped engineering of bipolar diketopyrrolopyrrole based small electron acceptor molecules for high performance organic solar cells*, 1201 (2021) 113242.
43. Mehboob, M.Y., et al., *Designing N-phenylaniline-triazol configured donor materials with promising optoelectronic properties for high-efficiency solar cells*, 1186 (2020) 112908.

Figures

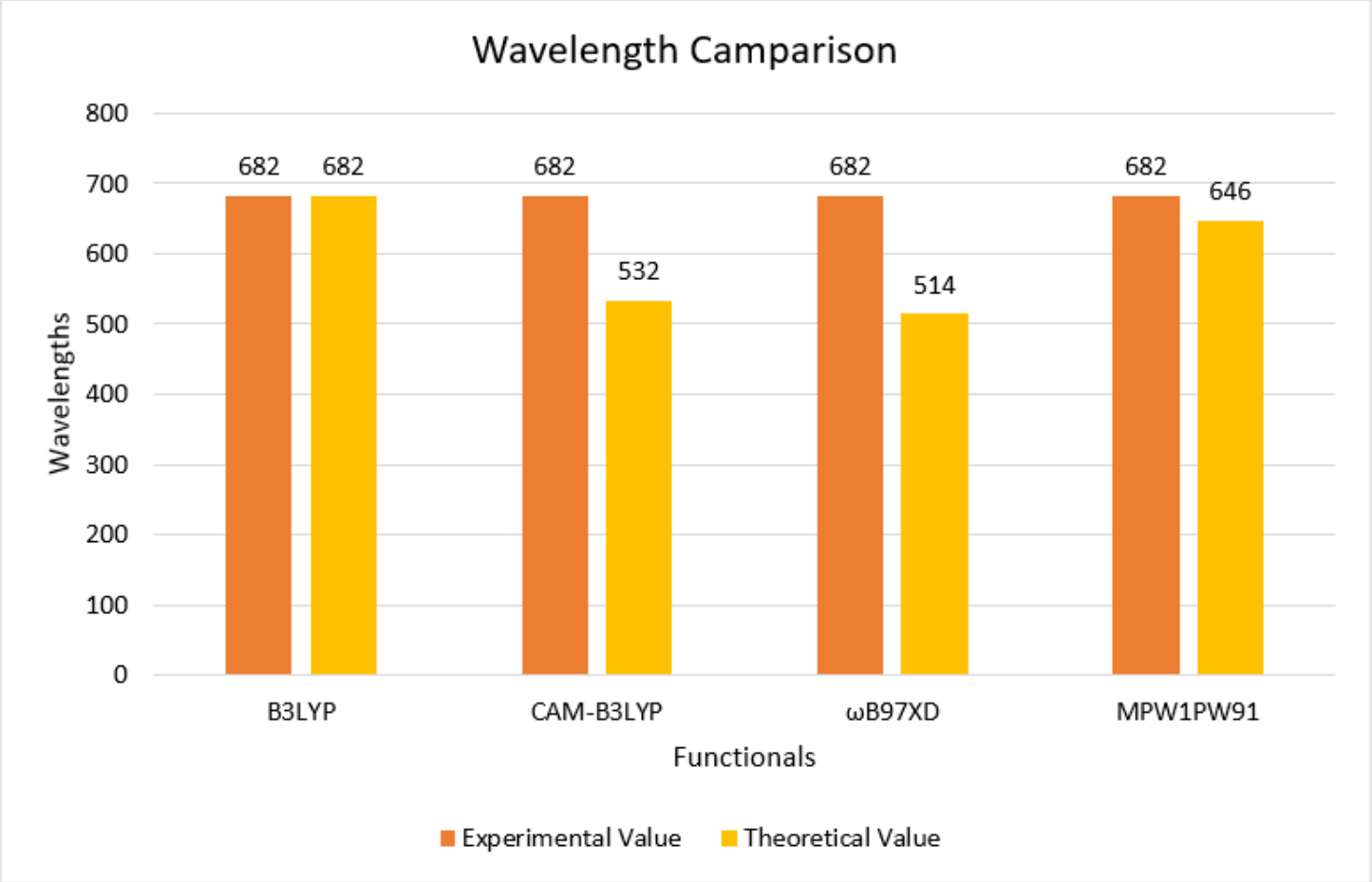

Figure 1

Column Chart showing comparison of λ_{max} obtained experimentally and at four Functional level B3LYP, CAM-B3LYP, ωB97XD, and MPW1PW91 using DFT with 6-31G (d,p) basis set

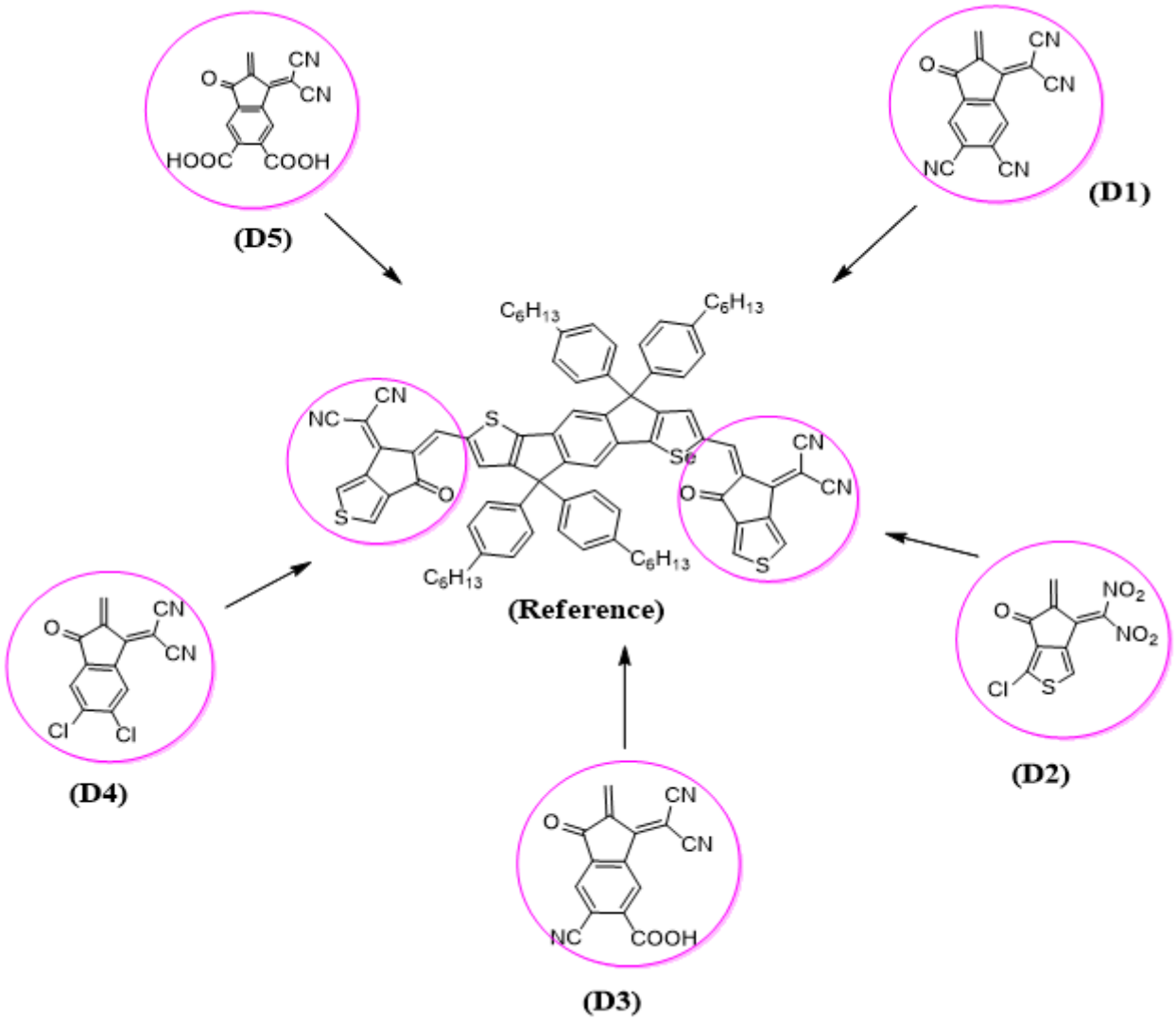

Figure 2

2D structure of Reference and newly fabricated terminal groups D1-D5

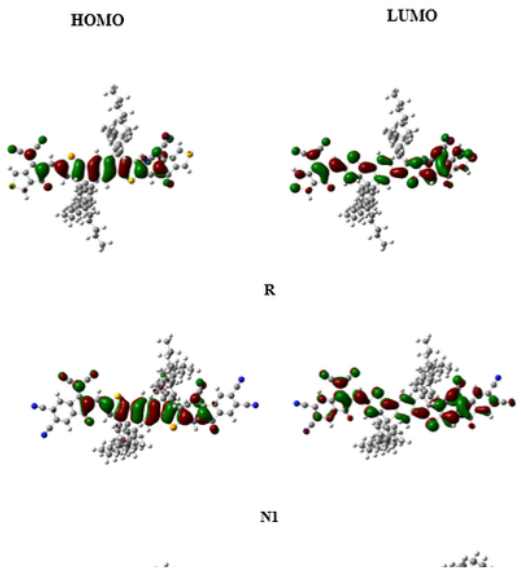

Figure 3

HOMO LUMO graphs of **R** and **N1-N5** applying DFT and 6-31G(d,p) level of DFT

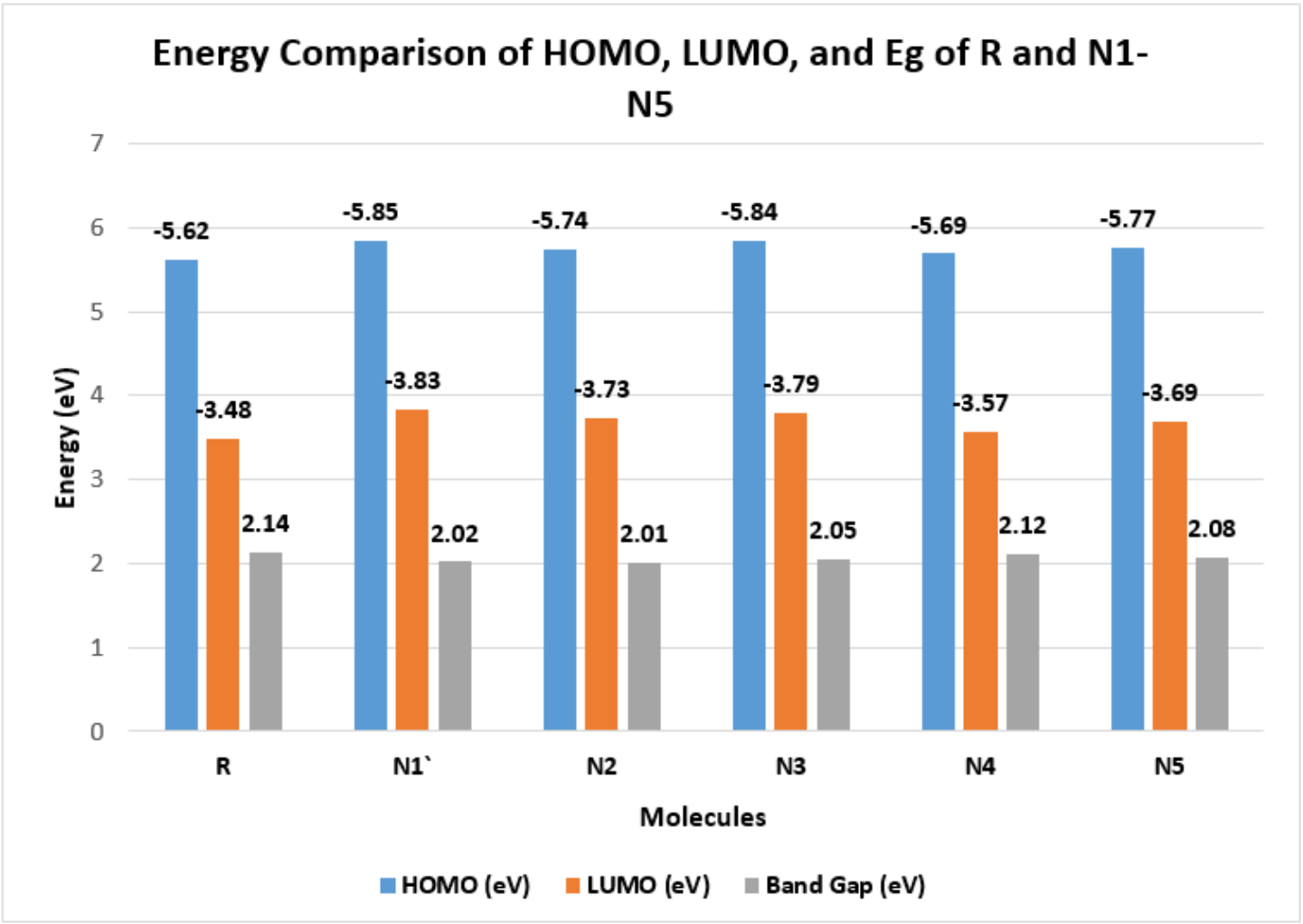

Figure 4

E_{HOMO}, E_{LUMO}, and energy band gap (E_g) of reference and newly designed molecules **N1-N5**

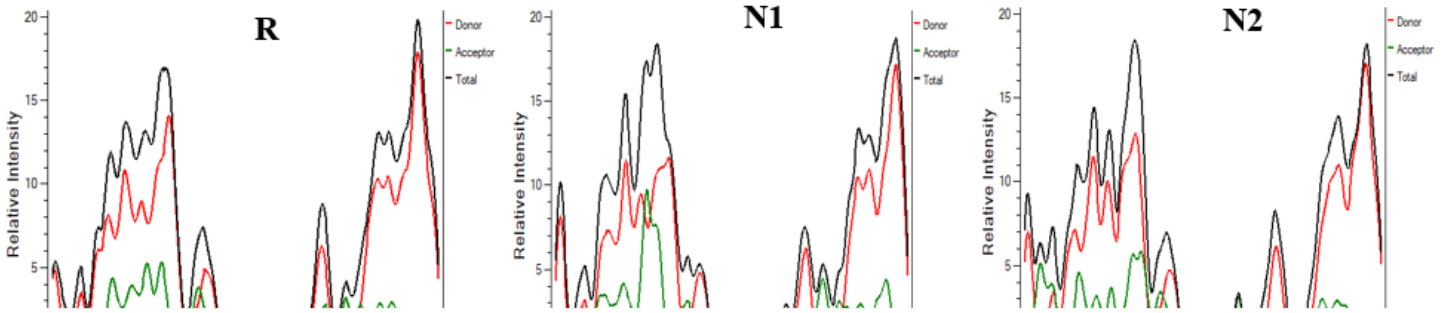

Figure 5

PDOS graphs of **R** and **N1-N5** calculated at B3LYP, 6-31G(d,p) level of DFT

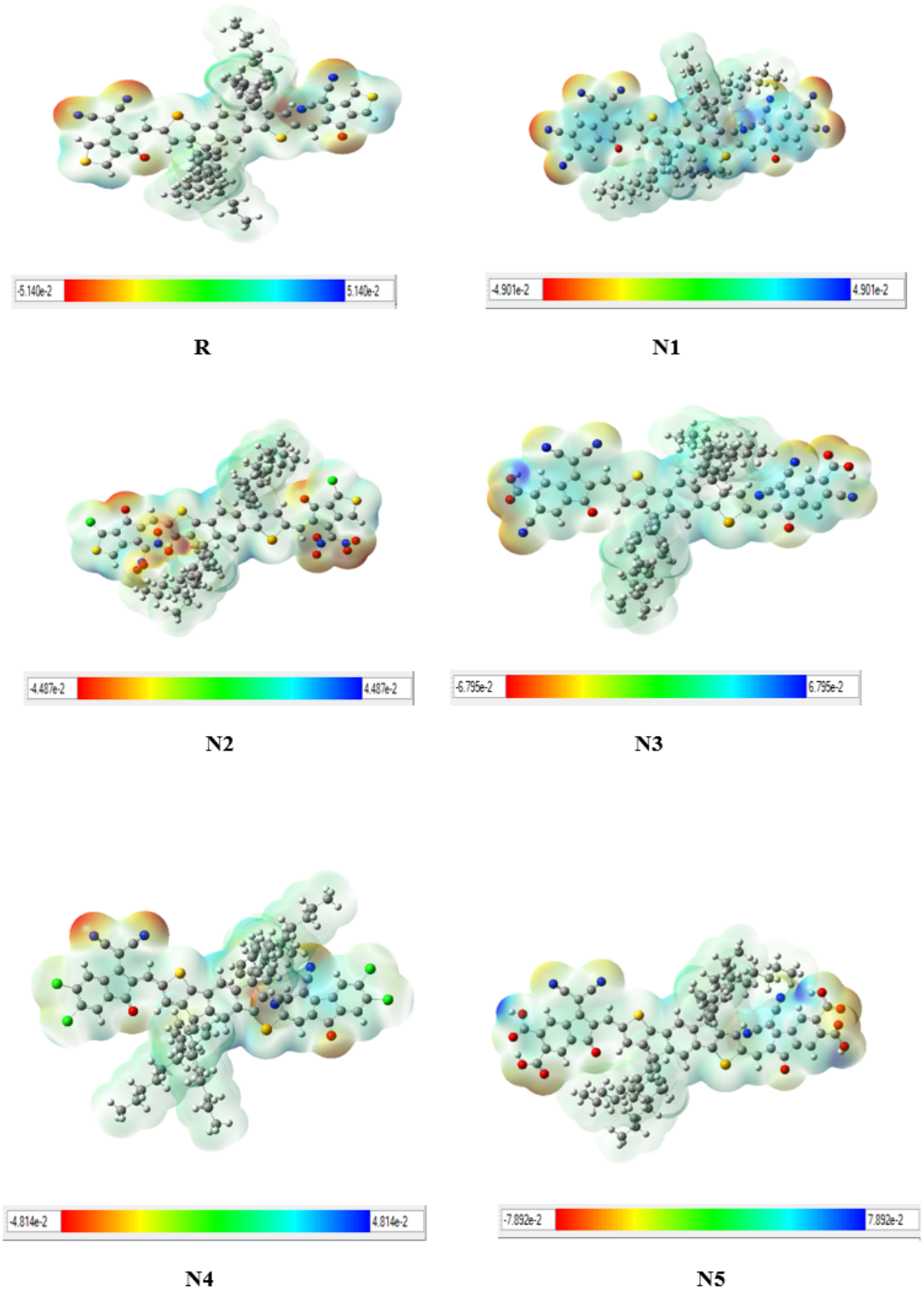

Figure 6

MEP plots of **R** and **N1-N5** applying DFT and basis set 6-31G(d,p)

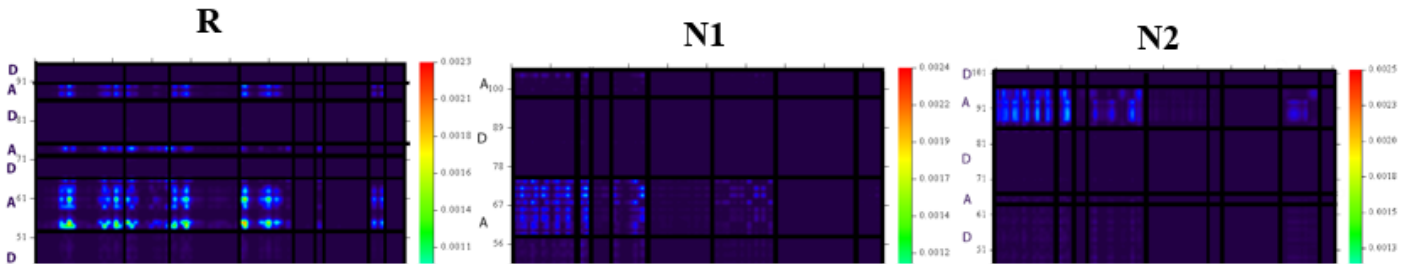

Figure 7

TDM graphs of **R** and **N1-N5** calculated at B3LYP and DFT level

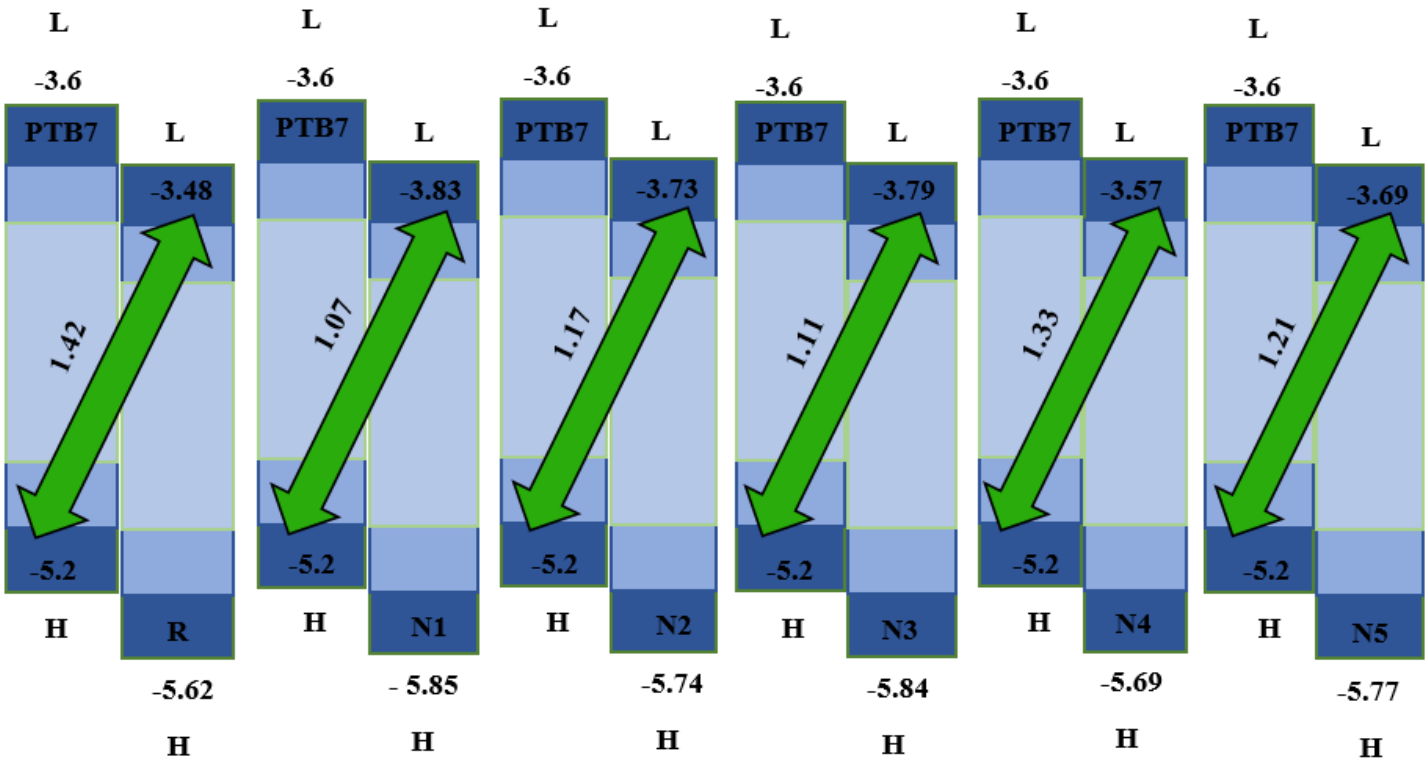

Figure 8

Systematically calculated open circuit values of reference and newly fabricated molecules **N1-N5**

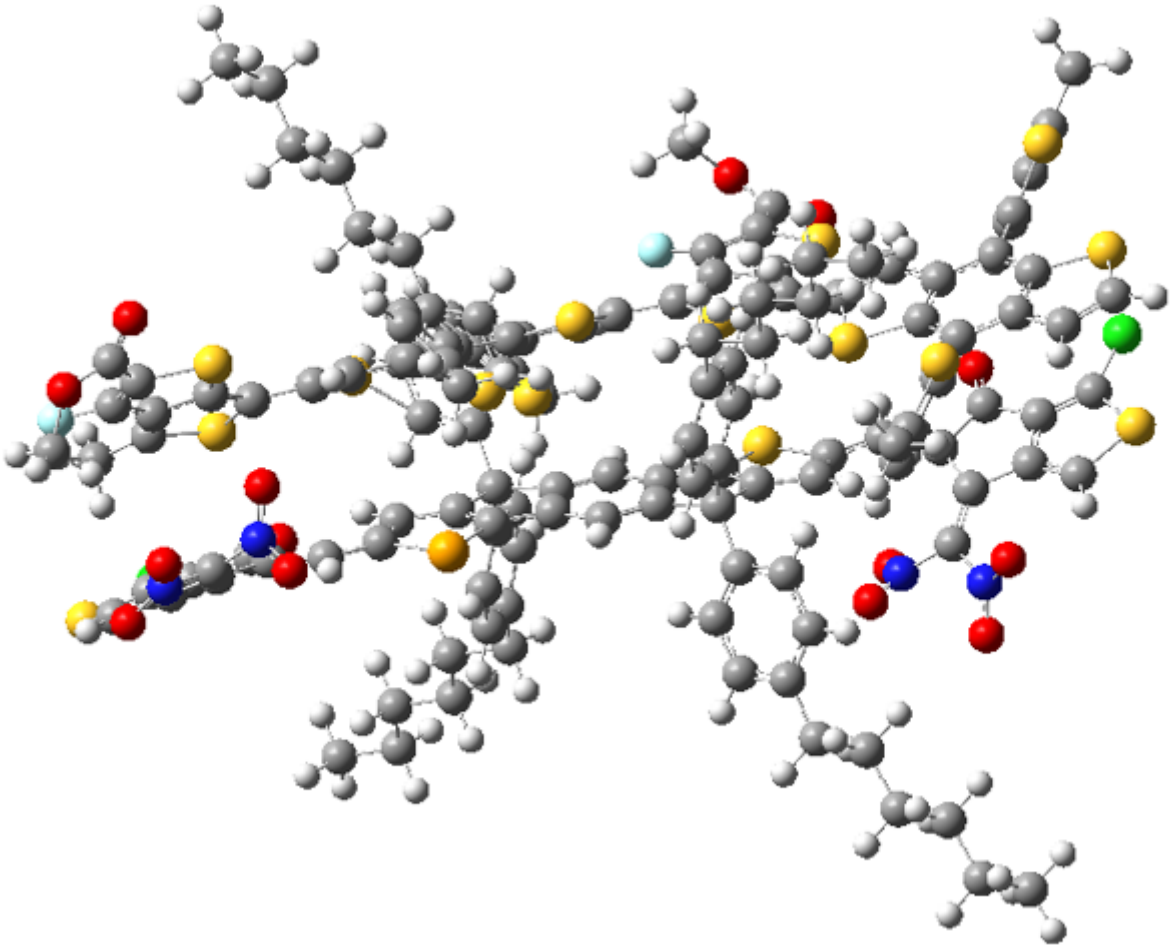

Figure 9

Optimized complex of **N2** with **PTB7-Th**

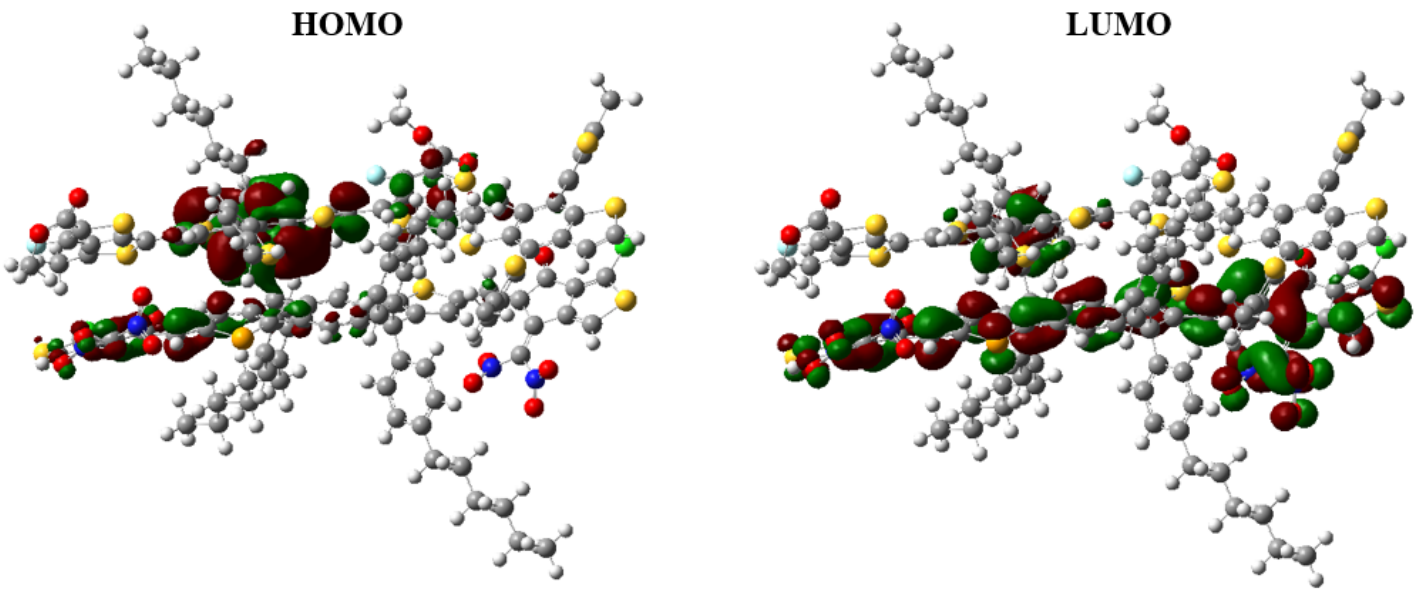

Figure 10

HOMO, LUMO graphs **N2** complex with **PTB7-Th**

Supplementary Files

This is a list of supplementary files associated with this preprint. Click to download.

- Supplementaryinformationfile.docx